Dynamic Tire/Soil Contact Surface Interaction Model for Aircraft Ground Operations

W. S. Pi*
Northrop Corporation, Hawthorne, California

This paper describes a dynamic tire/soil contact surface interaction model for aircraft ground operations. The formulation used a finite-element kernel function approach. It is based on the concept of the quasisteady motion of a tired wheel rolling at a constant speed on a linear viscoelastic layer (soil). In the soil model, the Young's modulus, Poisson's ratio, and shear modulus are treated as three independent parameters, and the inertia and viscous damping effects are included. The model thus developed can be utilized to predict the contact pressure distribution, soil deformation pattern, and tire footprint area shape developed beneath the moving tired wheel. Numerical examples were given to correlate the experimental results from a high-flotation test program. In general, the predicted drag ratio vs the speed results compare well with the test data trend for soils with various strengths. The analyses indicate that the high drag force and severe rutting occur when the wheel forward speed is near the shear wave velocity of the soil. Furthermore, the numerical results show that all soil parameters used in the model play significant roles in determining the soil strength and the responses. These parameters should be retained in a comprehensive analysis on aircraft tire/soil interaction.

I. Introduction

UNDER certain conditions, it is essential for an aircraft to be able to operate from unpaved soil fields. To insure acceptable ground operational performances in this adverse environment, mathematical models are created to simulate the aircraft responses. One important link of this simulation is the detailed interaction model involving the aircraft landing gear tire and the soil surface.

For the performance of an individual aircraft landing gear tire on soil fields, a large amount of test data is available in the literature (e.g., Ref. 1). Experiments have shown that the variations of the drag and rutting vs the tired wheel speed are complicated. In addition to the high drag and rutting values at near-static conditions, the corresponding values at high speeds usually exceed greatly those encountered at low speeds. Figure 1, adapted from Ref. 1, shows the experimental curves of the drag ratio (drag/vertical load analogous to friction coefficient) vs the aircraft speed from a Boeing high-flotation test program conducted in 1964.[1] The different California Bearing Ratio (CBR) values shown in Fig. 1 reflect the soil strength variation.

There have been few efforts to generate a practical landing gear tire/soil model to predict analytically the interaction behavior. The landing gear wheel tire/soil interaction model developed at Lockheed-Georgia,[2] by extending the Boeing Company's work,[1] is the only complete model available in the aircraft industry. The model was based upon the empirical load-deflection of the soil developed from the U.S. Army Waterways Experiment Station (WES). It consists of a discrete three-element solid viscoelastic system to simulate the basic soil behavior and uses additional correction terms to match the trend of test results on the inter-relationships among rut depth, drag load, and wheel speed. The model assumes point-contact between tire and soil. Thus, no contact pressure distribution information is provided. Recently, Cook developed a model with a number of discrete tire/soil elements for rough soil surfaces.[3] The soil element consists of a linear spring and a linear damper in series. It represents an attempt to model the complex soil characteristics with only two parameters.

This model can be applied to predict the drag ratio as well as the soil sinkage for a pneumatic tired wheel rolling at various constant speed on a semiprepared soil field with prescribed strength. Also predicted are the pressure distribution and soil deformation pattern developed beneath the tire, the shape of the tire footprint area, and the resultant vertical force, drag force, and moment acting on the wheel axle. As will be shown later, the predicted results match the test data trend over a wide range of aircraft taxi speed.

II. General Approach

The dynamic tire/soil contact surface interaction model developed in this paper is based on the concept of the quasisteady motion of a tired wheel rolling at a constant speed on a linear viscoelastic layer (soil), which leads to a finite, time-dependent deformation solution. The stress-strain behavior of the soil is simulated by a standard three-element solid model, consisting of a Maxwell spring and a Kelvin element (spring and dashpot in parallel) in series. The characteristics of the soil used in this approach are defined by the following parameters: E = Maxwell spring modulus (equivalent to the Young's modulus), E_2 = spring modulus of the Kelvin element, g = viscous damping constant, G = shear modulus, h = effective soil layer thickness, $\gamma = (E_2/\eta_2)$ for unloading, η_2 = viscosity coefficient of the dashpot of the Kelvin element, v = Poisson's ratio, and ρ = mass density.

For the soil model, the Young's modulus, Poisson's ratio, and shear modulus are treated as three independent parameters because of the relatively low value of G. However, the creep curves for compression and shear are assumed to be similar. For the recovery curves during unloading, a parameter γ that may be different from E_2/η_2 for loading is used because of the nature of the soil. The soil inertia and viscous damping effects are included in the formulation due to the

Presented as Paper 85-0708 at the AIAA/ASME/ASCE/AHS 26th Structures, Structural Dynamics and Materials Conference, Orlando, FL, April 15–17, 1985; received March 10, 1987; revision received July 6, 1987.

*Senior Technical Specialist, Aircraft Division, Dynamics and Loads Research Department. Associate Fellow AIAA.

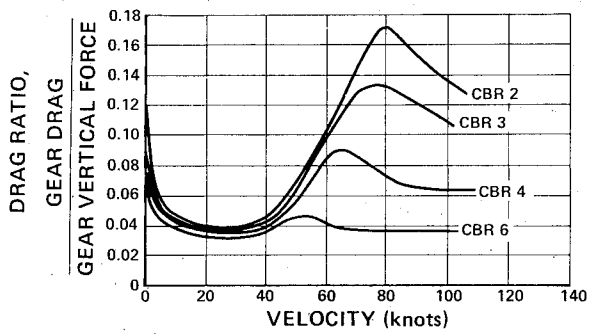

Fig. 1 Effect of velocity on the main-gear drag ratio from a high-flotation test program (Harper Lake Tests).

potentially high speed (e.g., 100 knots) considered in the landing/takeoff problems.

As will be described later, the averaged cone index CI, which was developed by the WES of the Corps of Engineers for the purpose of estimating soil strength, may be calculated as a function of E, v, G, E_2, and h from the stress-strain functions of the given soil model.[4] Thus, the equivalent soil layer thickness h may be computed whenever the experimentally determined values of E, v, G, E_2, and CI are available. It is important to note that the reverse process, i.e., the calculation from the CI to define the soil characteristics, is not possible. The measurement of E, v, G, E_2, and η_2 should be conducted under a loading condition equivalent to an average aircraft tire load value.

The present model uses a finite-element kernel function approach to evaluate the tire/soil interaction. The tire is simulated by a number of independent nonlinear spring elements along selected wheel radii.[5] The tire footprint area on the soil is divided into the same number of elements (strips) in the longitudinal direction. Within each element, the vertical force on the tire spring is equal to the product of the local contact pressure multiplied by the soil element area. The local tire width, or the soil element width, is a function of local tire vertical deformation.

The analytical formulation starts with the derivation of the kernel functions for the soil model using the linear viscoelastic theory based on the plane strain assumption. The kernel functions are defined as normal deformations of the viscoelastic layer (soil) subject to unit-concentrated normal and tangential surface loads moving with a constant speed. The final integral equation applying the kernel functions G_1 and G_2 for loading is as follows:

$$\int_0^{\ell} \{G_1(x-\xi) + \mu(\xi)G_2(x-\xi)\}p(\xi)\,d\xi = z(x) \tag{1}$$

where G_1 = normal soil surface deformation due to a unit-concentrated normal load moving with a constant speed, G_2 = normal soil surface deformation due to a unit-concentrated shear load moving with a constant speed, ℓ = length of the contact interval or the tire footprint length, p = contact pressure, z = soil normal deformation, and μ = surface friction coefficient, including the friction coefficient due to soil deformation.

By relating the contact pressure in Eq. (1) to the tire vertical load, and the soil deformation to the tire vertical deflection for each element, a set of simultaneous equations for the element contact pressures was established, covering the area of tire/soil contact. An iteration process was designed to reach a convergent solution for this nonlinear tire/soil interaction problem. In the following section, the detailed formulation for the kernel functions of the tire/soil interaction problem is described.

III. Soil Model

As discussed previously, the time-dependent stress-strain behavior of the soil is simulated by a standard three-element solid viscoelastic model. For the viscoelastic bodies, it can be assumed that the volume strain is purely elastic and the volume after-effect is neglected.[6] Thus, the strain-stress relationships for the state of plane strain may be expressed as

$$\sigma_x(t) = \frac{E(1-v)}{(1+v)(1-2v)}\left\{\varepsilon_x(t) + \frac{v}{1-v}\varepsilon_y(t) - m\int_{-\infty}^{t} e^{-n(t-\zeta)}[\varepsilon_x(\zeta) - \tfrac{1}{2}\varepsilon_y(\zeta)]\,d\zeta\right\} \tag{2}$$

$$\sigma_y(t) = \frac{E(1-v)}{(1+v)(1-2v)}\left\{\frac{v}{1-v}\varepsilon_x(t) + \varepsilon_y(t) - m\int_{-\infty}^{t} e^{-n(t-\zeta)}[-\tfrac{1}{2}\varepsilon_x(\zeta) + \varepsilon_y(\zeta)]\,d\zeta\right\} \tag{3}$$

$$\tau_{xy}(t) = 2G\left[\gamma_{xy}(t) - \frac{3(1-v)m}{2(1-2v)}\int_{-\infty}^{t} e^{-n(t-\zeta)}\gamma_{xy}(\zeta)\,d\zeta\right] \tag{4}$$

where $m = E/\eta_2$ and $n = (E + E_2)/\eta_2$.

The equilibrium equations and strain equations of the soil model take the forms of

$$\frac{\partial\sigma_x}{\partial x} + \frac{\partial\tau_{xy}}{\partial y} = \rho\frac{\partial^2 u}{\partial t^2} + c\frac{\partial u}{\partial t} \tag{5}$$

$$\frac{\partial\sigma_y}{\partial y} + \frac{\partial\tau_{xy}}{\partial x} = \rho\frac{\partial^2 v}{\partial t^2} + c\frac{\partial v}{\partial t} \tag{6}$$

$$\varepsilon_x = \frac{\partial u}{\partial x} \tag{7}$$

$$\varepsilon_y = \frac{\partial v}{\partial y} \tag{8}$$

$$\gamma_{xy} = \tfrac{1}{2}\left(\frac{\partial u}{\partial y} + \frac{\partial v}{\partial x}\right) \tag{9}$$

where c is the soil viscous damping coefficient, which is related to soil viscous damping constant g. Consider the elementary solution in the form of

$$\sigma_x = e^{i\beta x}\bar{\sigma}_x(\beta, y), \text{ etc.} \tag{10}$$

Substituting Eq. (10) into Eqs. (3–9) and transferring to a moving coordinate system with speed V, one can reduce the system of equations to one ordinary differential equation:[6]

$$C_1\frac{\partial^4\bar{\sigma}_y}{\partial y^4} + C_2\beta^2\frac{\partial^2\bar{\sigma}_y}{\partial y^2} + C_3\beta^4\bar{\sigma}_y = 0 \tag{11}$$

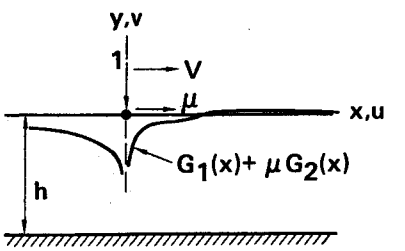

Fig. 2 Moving coordinate system of the soil model.

where

$$A=\frac{1-v}{(1+v)(1-2v)}(1-\bar{R})$$

$$B=\frac{1-v}{(1+v)(1-2v)}\left(\frac{v}{1-v}+\tfrac{1}{2}\bar{R}\right)$$

$$C=\frac{2G}{E}\left[1-\frac{3(1-v)}{2(1-2v)}\bar{R}\right]$$

$$C_1=AC$$

$$C_2=2BC+2B^2-2A^2+NC+2NA$$

$$C_3=(A-N)(C-2N)$$

$$N=\rho V^2(1+ig)/E$$

$$\bar{R}=m/(n-i\beta V)$$

and the soil viscous damping coefficient c in Eqs. (5) and (6) is approximated by the term $\rho g V\beta$.

Let

$$\sigma_y=\sum_{k=1}^{4}Q_k e^{\lambda_k\beta y} \tag{12}$$

the roots of the characteristic Eq. (11) are

$$\lambda_1=-\lambda_3=-\left[\frac{1}{2C_1}(-C_2+\sqrt{C_2^2-4C_1C_3})\right]^{\frac{1}{2}}$$

$$\lambda_2=-\lambda_4=-\left[\frac{1}{2C_1}(-C_2-\sqrt{C_2^2-4C_1C_3})\right]^{\frac{1}{2}} \tag{13}$$

For the case $G=E/2(1+v)$, Eq. (13) can be reduced to

$$\lambda_1=-(1-N/A)^{\frac{1}{2}}$$

$$\lambda_2=-(1-2N/C)^{\frac{1}{2}} \tag{14}$$

The solution of the boundary-value problem may be obtained by substituting Eq. (12) into the following expressions for $\bar{\tau}_{xy}$, $\bar{u}$, and $\bar{v}$:[6]

$$\bar{\tau}_{xy}=\frac{iC}{C_7}\left(C_5\beta^{-1}\frac{\partial\bar{\sigma}_y}{\partial y}+C_6\beta^{-3}\frac{\partial^3\bar{\sigma}_y}{\partial y^3}\right) \tag{15}$$

$$\bar{v}=-\frac{1}{EN}\left(\beta^{-2}\frac{\partial\bar{\sigma}_y}{\partial y}+i\beta^{-1}\bar{\tau}_{xy}\right) \tag{16}$$

$$\bar{u}=\frac{i}{E(A+B)(A-B-N)}\left[A\beta^{-3}\frac{\partial^2\bar{\sigma}_y}{\partial y^2}+(B+N)\beta^{-1}\bar{\sigma}_y\right] \tag{17}$$

where

$$C_5=A^2-B^2-2NB-NA-N^2$$

$$C_6=-NA$$

$$C_7=(C-2N)(A+B)(A-B-N)$$

The boundary conditions used for the kernel function determination are

$$\left.\begin{aligned}\sigma_y&=-\delta(x)\\ \tau_{xy}&=\mu\delta(x)\end{aligned}\right\}\quad(y=0,\ -\infty<x<\infty) \tag{18, 19}$$

$$\left.\begin{aligned}u&=0\\ v&=0\end{aligned}\right\}\quad(y=-h,\ -\infty<x<\infty) \tag{20, 21}$$

where δ is a delta function and μ the surface friction coefficient. See Fig. 2 for the sign convention.

The elementary solution of the normal deformation of the viscoelastic layer $\bar{v}(\beta,0)$ can be then expressed in the following form:

$$\bar{v}(\beta,0)=\frac{-1}{E\beta\,\Delta}\{(\beta_1\alpha_2-\alpha_1\beta_2)(\gamma_1\alpha_2D_1S_2-\gamma_2\alpha_1S_1D_2)+i\mu[(\gamma_1+\gamma_2)\alpha_1\alpha_2(D_1D_2-1)-(\gamma_2\alpha_1^2+\gamma_1\alpha_2^2)S_1S_2]\} \tag{22}$$

where

$$D_j=\cosh(\lambda_j\beta h),\qquad j=1,2$$

$$S_j=\sinh(\lambda_j\beta h),\qquad j=1,2$$

$$\alpha_j=-\frac{1}{NC_7}\lambda_j[C_7-C(C_5+\lambda_j^2)C_6],\qquad j=1,2$$

$$\beta_j=\lambda_j+\alpha_jN,\qquad j=1,2$$

$$\gamma_j=A\lambda_j^2+B+N,\qquad j=1,2$$

$$\Delta=-(\gamma_2\beta_1\alpha_2+\gamma_1\beta_2\alpha_1)+(\gamma_1\beta_1\alpha_2+\gamma_2\beta_2\alpha_1)D_1D_2-(\gamma_2\beta_1\alpha_1+\gamma_1\beta_2\alpha_2)S_1S_2$$

The normal deformation of the soil layer in the spatial domain can be evaluated by the expression

$$v(x)=\frac{1}{\pi}Re\int_0^\infty\bar{v}(\beta,0)e^{i\beta x}\,d\beta \tag{23}$$

To evaluate Eq. (23), the following two limiting cases of the elementary solution $\bar{v}(\beta,0)$ are examined:

$$\beta\to 0,\qquad \bar{v}\to\frac{-h}{EA} \tag{24}$$

This indicates that the normal deformation v will approach infinity if the soil layer is extended to a half space (i.e., h approaches to infinity).

β is large such that $|\bar{R}|\ll 1$ and $D_j\cong -S_j\gg 1$,

$$\bar{v}\to\frac{1}{E\beta(\beta_1-\beta_2)}[\beta_1\alpha_2-\alpha_1\beta_2+i\mu(\alpha_2-\alpha_1)] \tag{25}$$

Rewrite Eq. (25) in the form of

$$\bar{v}\to\frac{-1}{E\beta}\frac{(p_1+p_2\bar{R})}{(q_1+q_2\bar{R})} \tag{26}$$

Eq. (26) can be approximated by the following expressions:

$$\bar{v}\to\bar{v}_\infty+\bar{v}_{\infty 0} \tag{27}$$

$$\bar{v}_\infty=-\left(r_1+\frac{m}{n}r_2\right)/E\beta \tag{28}$$

$$\bar{v}_{\infty 0}=-iV\bar{R}r_2/En \tag{29}$$

where

$$r_1 = p_1/q_1$$

$$r_2 = (p_2 - r_1 q_2)/q_1$$

Based on the behavior of the asymptotic expression of $\bar{v}$, the integral in Eq. (23) can be carried out in the following manner:

$$v(x) = v_1(x) + v_2(x) + v_3(x) \tag{30}$$

$$v_1(x) = \frac{1}{\pi} Re \int_0^{\beta_c} (\bar{v} - \bar{v}_{\infty 0}) e^{i\beta x}\, d\beta \tag{31}$$

$$\begin{aligned} v_2(x) &= \frac{1}{\pi} Re \int_{\beta_c}^{\infty} \bar{v}_{\infty} e^{i\beta x}\, d\beta \\ &= \frac{1}{E\pi}\left\{ Re\left(r_1 + \frac{m}{n} r_2\right) Ci(\beta_c |x|) \right. \\ &\quad \left. - Im\left(r_1 + \frac{m}{n} r_2\right) Si(\beta_c |x|) \frac{x}{|x|} \right\} \end{aligned} \tag{32}$$

$$\begin{aligned} v_3(x) &= \frac{1}{\pi} Re \int_0^{\infty} \bar{v}_{\infty 0} e^{i\beta x}\, d\beta \\ &= \frac{m}{E\pi n} e^{nx/V} \left\{ -Re\, r_2 Ei\left(-\frac{nx}{V}\right) + Im\, r_2 \pi H(-x) \right\} \end{aligned} \tag{33}$$

where *Ci*, *Si*, and *Ei* are the cosine integral, sine integral, and exponential integral function, respectively. H is a step function, and β_c is the lower bound of β, such that Eqs. (27–29) are valid. The term $v_1(x)$ in Eq. (31) is obtainable by numerical integration.

Rewriting $v(x)$ as

$$v(x) = -\{G_1(x) + \mu G_2(x)\} \tag{34}$$

G_1 and G_2 are then the kernel functions of the dynamic tire/soil contact surface interaction model in Eq. (1) due to normal and shear load, respectively. Both G_1 and G_2 feature singularity $\ell n\, x$ and discontinuity at $x = 0$.

IV. Soil Strength Determination

The cone index C_{WES} has been used in the prediction of soil strength.[4] It is defined as twice the force required for a 30-deg cone having a 0.5-in.^{2} base area to penetrate the top soil layer and is a function of soil sinkage.[4] There is a certain relationship existing between the CBR and the averaged CI. For the Harper Lake soil (Fig. 1), a ratio of CBR to CI of 1 to 40 was used.[1] The WES of the Corps of Engineers has developed a method to calculate the CI with acceptable accuracy from the appropriate empirically defined stress-strain function of the given terrain. The same method can be applied to calculate the CI, $C_{WES}(z)$ based on the stress-strain relationship of the present soil model. Let CI be the averaged value of C_{WES} up to 6 in. of sinkage. It is clear that CI is a function of E, G, ν, E_2, and h. Thus, with given values of E, G, ν, E_2, and CI, the equivalent soil layer thickness can be determined.

V. Tire/Soil Interaction

For aircraft ground operation applications, the multispring tire model developed by Cook and Ingram[3,5] is employed to interact with the derived soil model. The tire model uses a number of nonlinear independent spring elements along selected wheel radii to represent the tire, as shown in Fig. 3. For each tire element, the tire element force f_j is expressed in terms of tire spring displacement ε_j in the following form:

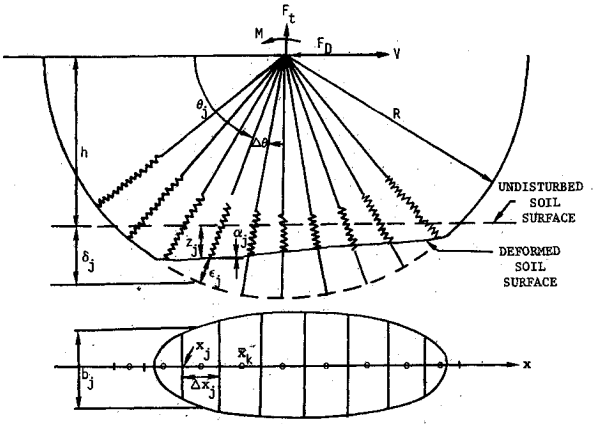

Fig. 3 Tire/soil interaction model.

$$f_j = (Q_1 \varepsilon_j + Q_2 \varepsilon_j^2) H(\varepsilon_j) \tag{35}$$

where Q_1 and Q_2 are the tire spring constants to be determined based on the tire load-deflection curve for the tire on a rigid flat surface by a least-squares fit.

For this tire model, the axle vertical force F_t and drag force F_D may be represented by

$$\begin{aligned} F_t &= \sum_{j=1}^{N} f_{vj} \\ &= \sum_{j=1}^{N} (Q_1 \varepsilon_{vj} + Q_2 \varepsilon_{vj}^2 / \sin\theta_j) \end{aligned} \tag{36}$$

$$F_D = \sum_{j=1}^{N} (\mu_0 + \tan\alpha_j - \cot\theta_j) f_{vj} \tag{37}$$

where f_{vj} = vertical tire spring element force, N = total number of tire elements in contact with the soil, α_j = local slope of the deformed tire/soil surface, ε_{vj} = vertical component of the tire element displacement, θ_j = inclination angle of the tire element spring (Fig. 3), and μ_0 = friction coefficient between the tire and rigid surface. The contact pressure distribution in the lateral direction ξ of the tire footprint area (Fig. 3) is assumed in the form of

$$p(x,\xi) = \bar{p}(x) F(2\xi/b) \tag{38}$$

where F is a given shape function and b is the local tire footprint width.

The tire footprint area on the soil is divided into the same number of strips corresponding to the tire elements in the longitudinal direction (Fig. 3). Within each element, the vertical tire spring element force is equal to the resultant force on the corresponding soil element,

$$f_{vj} = p_j b_j \Delta x_j \bar{F} \tag{39}$$

where p_j is the average contact pressure intensity at $\xi = 0$, b_j is the local tire footprint width, Δx_j is the soil element length, and $\bar{F}$ is defined as

$$\bar{F} = 2 \int_0^{b/2} F(2\xi/b)\, d\xi \tag{40}$$

The tire width b_j is approximated by a function of the undeflected tire width b_0 and the local tire vertical displacement ε_{vj}:

$$b_j = b_0 [1 - (1 - 2\varepsilon_{vj}/b_0)^2]^{1/2} \tag{41}$$

For this finite-element tire/soil interaction model, the soil deformation z_k can be expressed in terms of the kernel functions and the contact pressure p in the following form:

$$z_k = \sum_{j=1}^{N} G_{kj} p_j \tag{42}$$

where

$$G_{kj} = \int_{x_j}^{x_{j+1}} [G_1(\bar{x}_k - \zeta) + (\mu_0 + \tan\alpha_j - \cot\theta_j) G_2(\bar{x}_k - \zeta)]\, d\zeta$$

provided that the tire element is in contact with soil, i.e., $\varepsilon_{vj} > 0$ (Fig. 3).

For a given wheel axle position and the undisturbed soil surface profile, the compatibility condition in displacement yields the relationship between the local vertical tire deflection and soil deformation (Fig. 3) as follows:

$$\varepsilon_{vk} + z_k = \delta_k = R \sin\theta_k - h \tag{43}$$

where R is the undeflected tire radius and h is the vertical displacement between the wheel axle and undisturbed soil surface. With the aid of Eqs. (35), (39), (42), and (43), a set of equations to be satisfied by the local pressures can be established in the following form:

$$\bar{F} b_k \Delta x_k p_k = Q_1\left(\delta_k - \sum_j G_{kj} p_j\right) + Q_2\left(\delta_k - \sum_j G_{kj} p_j\right)^2 / \sin\theta_k \tag{44}$$

Because of the nonlinear nature of the problem, an iteration process is required to solve the unknowns. Knowing the converged values of p_k and b_k, the soil deformation pattern, soil sinkage z_s (deformation at the trailing edge of the tire footprint length), and axle loads (vertical force F_t, drag force F_D, and moment M) can be determined.

For a given vertical load applied to the wheel axle, a one-dimensional search process is needed to solve the problem. The soil deformation under the wheel axle is usually selected as the design variable.

For unloading, the soil deformation recovery curve (rutting) may be represented by the following equation:

$$z_r(t_r) = z_s \exp(-\gamma t_r) \tag{45}$$

where t_r is the unloading time. When γ approaches zero, there is a permanent rut depth that equals the soil sinkage z_s.

VI. Numerical Examples

Numerical examples were set up to correlate the test results on the drag ratio vs the speed relationship, as illustrated in Fig. 1. The data in Fig. 1 were measured during the high-flotation tests performed by a Boeing 367-80 airplane,[1] while the values predicted by the present tire/soil interaction model are under a given vertical load condition.

The physical properties of the soil used in the examples are listed in Table 1. Also listed are the shear wave velocity $V_s = \sqrt{G/\rho}$ for the soil corresponding to an unbounded elastic medium. The CI values of 80, 120, 160, and 240 are equivalent to CBR values of 2, 3, 4, and 6 as values for the curves shown in Fig. 1, when a ratio of CBR to CI of 1 to 40 is used.[1] A set of CI vs h plots are depicted in Fig. 4.

The tire data used in the computation are the same as those used for the main gear tire of the Boeing 367-80 airplane. The

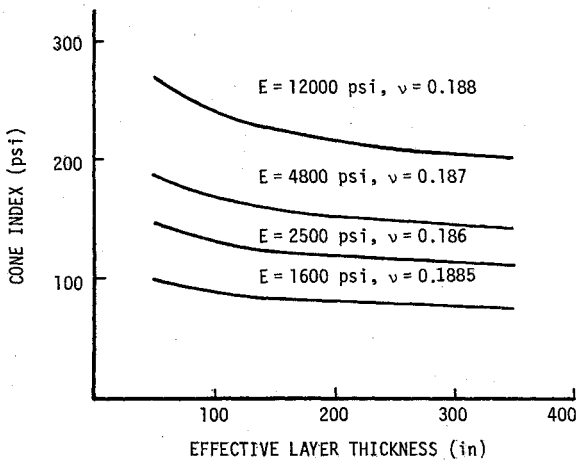

Fig. 4 Averaged cone index vs effective layer thickness plot for $E_2/E = 1.0$.

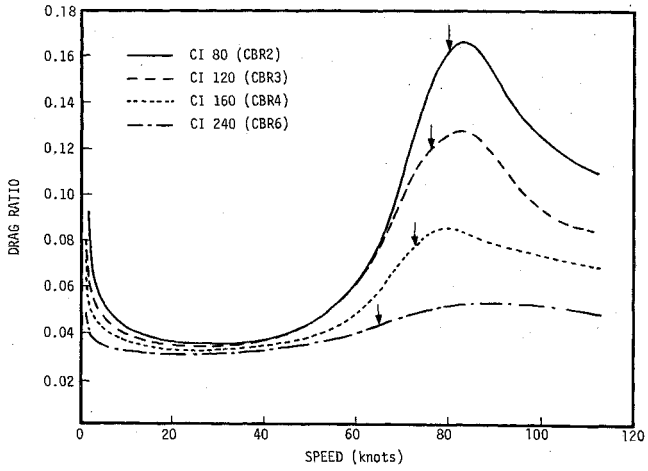

Fig. 5 Predicted drag ratio F_D/F_t vs forward speed plot, $F_t = 9300$ lb.

Table 1 Physical properties of soil

Soil Parameter	CI = 80 CBR = 2	CI = 120 CBR = 3	CI = 160 CBR = 4	CI = 240 CBR = 6
E (psi)	1600	2500	4800	12000
ν	0.1885	0.186	0.187	0.188
G (psi)	300	300	300	300
E_2/E	1	1	1	1
E/η_2 (1/s)	0.7	0.7	0.8	0.8
ρ (lb-s^2/in.^{4})	0.000114	0.000127	0.000138	0.000173
g	0.30	0.30	0.34	0.42
h (in.)	200	200	150	100
V_s (knot)	80.1	75.9	72.8	65.0

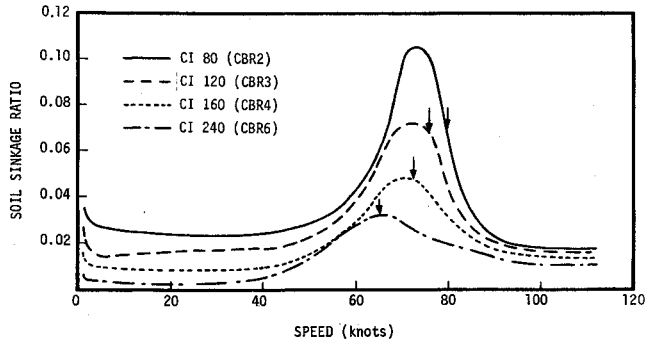

Fig. 6 Predicted soil sinkage ratio $z_s/2R$ vs forward speed plot, $F_t = 9300$ lb.

tire's outer radius R is 23 in., and the deflected tire's width b_0 is 16 in. These examples will predict the tire/soil responses for the tired wheel rolling on a flat soil surface under a 9300-lb vertical load. The friction coefficient μ_0 is assumed to be 0.33. The value of $\bar{F}$ in Eq. (44) is assumed to be unity.

The tire spring constants Q_1 and Q_2 in Eq. (35) were determined by a least-squares fit to match the tire load-deflection curve up to 3 in. of tire deflection using 15 tire spring elements. It yields

$$Q_1 = 369.5$$

$$Q_2 = -38.9$$

The result on tire load-deflection approximation is given in Table 2.

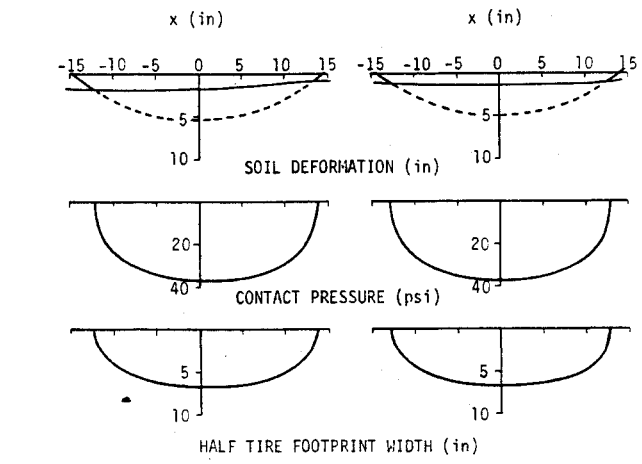

(a) V/V_s = 0.02; V = 1.6 knots; ℓ = 25.0 in; F_D = 861 lb; M = 6,168 in-lb; z_s = 1.65 in

(b) V/V_s = 0.30; V = 4.0 knots; ℓ = 26.0 in; F_D = 333 lb; M = 602 in-lb; z_s = 1.09 in

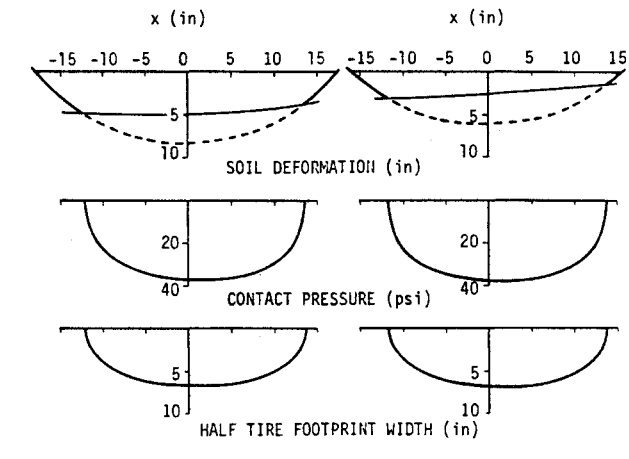

(c) V/V_s = 0.91; V = 72.9 knots; ℓ = 26.0 in; F_D = 1,178 lb; M = 9,291 in-lb; z_s = 4.81 in

(d) V/V_s = 1.0; V = 80.1 knots; ℓ = 26.0 in; F_D = 1,518 lb; M = 12,829 in-lb; z_s = 3.02 in

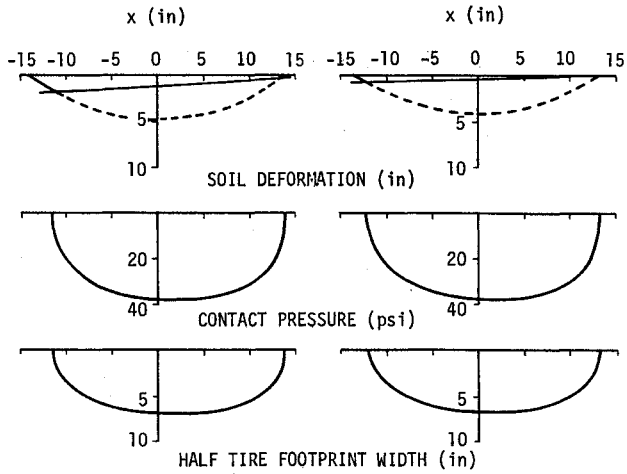

(e) V/V_s = 1.05; V = 84.1 knots; ℓ = 26.0 in; F_D = 1,550 lb; M = 13,511 in-lb; z_s = 1.71 in

(f) V/V_s = 1.4; V = 112.1 knots; ℓ = 25.0 in; F_D = 1,023 lb; M = 7,889 in-lb; z_s = 0.80 in

Fig. 7 Contact pressure distributions, soil deformation patterns, and half-tire footprint areas developed beneath the deformed tire on CI80 (CBR 2) soil, $F_t = 9300$ lb.

Table 2 Tire load-deflection approximation

Tire deflection (in.)	Tire vertical load (lb)	
	Manufacturer's value	Approximated value
0	0	0
1.215	2500.0	2293.7
2.235	5000.0	5154.9
3.0	7400.0	7381.1

The values of drag ratio predicted by the present tire/soil interaction model for various wheel forward speeds are plotted in Fig. 5. The nondimensional values of soil sinkage $z_s/2R$ vs the speed are given in Fig. 6. The arrowheads in Figs. 5 and 6 indicate the shear speed for each type of soil. Figure 5 illustrates that the trend of the predicted drag ratio results match well with the trend of the test data in Fig. 1 over a wide range of aircraft taxi speed for soil with various strengths. After the high drag ratio observed at near zero speeds, the drag ratio is reduced to a low level when the speed ratio V/V_s is in the range of 0.1 and 0.7. Then the drag ratio increases with the speed ratio until a peak value is reached with a speed ratio between 1.0 and 1.20. A similar trend is observed in the soil sinkage vs the speed plots in Fig. 6. The peak values of soil sinkage occur at the V/V_s value between 0.91 and 0.95. When the speed ratio exceeds 0.95, the soil sinkage decreases rapidly.

In Fig. 7, the contact pressure distribution, soil deformation pattern, and tire footprint area developed beneath the deformed tire on the CI 80 or CBR 2 soil are depicted for speed ratios of 0.02, 0.3, 0.91, 1.0, 1.05, and 1.4, respectively. The soil deformation pattern corresponding to zero speed (not shown) is symmetric with respect to the vertical plane containing the wheel axle. As the speed increases, the average soil deformation reduces, but the slope of the deformation surface increases to cause higher drag load (see Fig. 7a). In Fig. 7b, the deformation slope, corresponding to 0.3 speed ratio, is reduced to a minimum, and the drag ratio is only slightly higher than the value of $\mu_0(=0.03)$, the friction coefficient between the tire and a rigid surface. In Fig. 7c, $V/V_s = 0.91$, the soil sinkage is most severe, and the tire footprint length is relatively short. When $V = V_s$ (Fig. 7d), the steep deformation slope associated with less severe soil deformation, which results in a larger contact area, yields a high drag load. The soil deformation pattern in Fig. 7e, $V/V_s = 1.05$, shows that the soil sinkage is much lower, but the drag force is high because of the steep deformation slope. Figure 7f shows that at a higher speed, $V/V_s = 1.4$, the drag force is moderate, and there is almost no soil deformation in front of the tire. The dashed line in each plot of Fig. 7 reflects the shape of an undeflected tire.

VII. Conclusions

A dynamic tire/soil contact surface interaction model has been developed for aircraft to perform ground operations on semiprepared soil fields. The formulation is based on the concept of the quasisteady motion of a tired wheel rolling at a constant speed on a linear viscoelastic layer (soil) using a finite-element kernel function approach. In the soil model, the Young's modulus, Poisson's ratio, and shear modulus are treated as three independent parameters because of the relatively low value of the shear modulus. The soil inertia and viscous damping effects are included in the formulation because of the potentially high speeds considered in aircraft ground operations. To complete the analysis, a procedure was also established to calculate the CI, which represents the soil strength based on the soil parameter input. The model can be utilized to predict the contact pressure distribution, soil deformation pattern, and tire footprint area shape developed beneath the moving tired wheel on a soil field with prescribed strength.

This more elaborate tire/soil interaction model has been mechanized for numerical computations. Examples were given to correlate the experimental results from a high-flotation test program.[1] In general, the predicted drag ratio vs the speed results compare well with the test data trend over a wide range of aircraft taxi speeds for soils with various strengths. The analyses indicate that the high drag force and severe rutting occur when the wheel forward speed is near the shear wave velocity of the soil and the soil shear modulus is almost invariable with soil strength. Furthermore, the numerical results show that all soil parameters used in the model play significant roles in determining the soil strength and the responses. These parameters should be retained in a comprehensive analysis on aircraft tire/soil interaction.

The derived tire/soil interaction model can be linked to general aircraft landing/taxi response analysis computer codes for analytical simulations. The computer cost saving can be achieved by using fewer tire/soil elements and by interpolating the kernel functions among those corresponding to the key values of the speed ratio. This model can be extended to handle the rough soil field problem by inputting the local vertical displacement between the wheel axle and the undisturbed soil surface for each soil element. On the other hand, if the computation cost is not a problem, then the capability of the tire/soil interaction model can be enhanced for aircraft turning simulations by introducing additional elements in the lateral direction.

Acknowledgment

This work was supported by Northrop's Independent Research and Development program. The author acknowledges Dr. M. M. Ratwani for suggesting this problem.

References

[1]Richmond, L. D., Brueske, N. W., and Debord, K. J., et al., "Aircraft Dynamic Loads from Substandard Landing Sites," Part I, Summary, and Part II, Development of Tire-Soil Mathematical Model, Air Force Flight Dynamics Lab., TR-67-145, Boeing Co., Sept. 1968.

[2]Crenshaw, B. M., "Development of an Analytical Technique to Predict Aircraft Landing Gear/Soil Interaction," Air Force Flight Dynamics Lab., TR-74-115, Lockheed-Georgia Co., Jan. 1975.

[3]Cook, R. F., "Tire Model for Computing Axle Loads and Displacement from Short Wavelength Obstacles," UDR-TR-81-40, Univ. of Dayton Research Institute, March 1981.

[4]Janosi, Z., "Prediction of WES CONE INDEX by Means of a Stress-Strain Function of Soils," Rept. 46, Dept. of the Army Ordinance Tank-Automotive Command Research Div., Land Locomotive Laboratory, Feb. 1959.

[5]Ingram, W. F., "A Numerical Model of the Ride Dynamics of a Vehicle Using a Segmented Tire Concept," TRM-73-5, U.S. Army Water Ways Experiment Station, Aug. 1973.

[6]Galin, L. A. and Shmatkova, A. A., "Motion of a Rigid Stamp on the Boundary of a Viscoelastic Half-Plane," PMM, Vol. 32, No. 3, 1968, pp. 445–453.